

RESEARCH ARTICLE

[View Article Online](#)
[View Journal](#) | [View Issue](#)



Cite this: *Inorg. Chem. Front.*, 2025, **12**, 588

Novel antimony-based mixed halides exhibiting an excellent SHG response and a broad transmission range†

Luli Wang,^a Han Luo,^a Siyu Chen,^a Ling Huang,^{ID *a} Liling Cao,^{ID *a} Xuehua Dong^a and Guohong Zou^{ID *b}

In this study, we successfully synthesized two novel non-centrosymmetric (NCS) antimony halide compounds, **RbSbF₃Cl** and **Rb₃Sb₄F₁₄Cl**. These compounds were formed by combining Sb³⁺ cations, which possess stereochemically active lone pairs (SCALP), with halogen atoms (fluorine and chlorine). The introduction of mixed halogen atoms enables Sb atoms to adopt multiple coordination modes, which in turn promotes the development of both compounds towards NCS structures. Notably, **Rb₃Sb₄F₁₄Cl** demonstrated a large second harmonic generation (SHG) response, approximately three times greater than that of KH₂PO₄ (KDP), along with a wide transparency range from 0.27 to 13.3 μm and a high laser damage threshold (LDT) of 223 MW cm⁻². These exceptional properties indicate that **Rb₃Sb₄F₁₄Cl** is a highly promising nonlinear optical (NLO) crystal with excellent overall performance, making it suitable for potential applications spanning the short-wave ultraviolet (UV) to mid-infrared (IR) spectral regions. In contrast, **RbSbF₃Cl** exhibits a large birefringence of 0.31 at 546 nm as a uniaxial crystal, suggesting its practicability as a birefringent material.

Received 31st October 2024,
Accepted 4th December 2024

DOI: 10.1039/d4qi02757d

rsc.li/frontiers-inorganic

Introduction

Nonlinear optical (NLO) materials have significant academic and technological value in extending the wavelength range of solid-state lasers from deep ultraviolet (UV) (<200 nm) to infrared (IR) (~20 μm) through simple frequency conversion.^{1–6} From a commercial perspective, an ideal NLO crystal must possess several key characteristics, one of which is a broad transparent window, which determines the application range of the crystal.^{7–10} Over the past few decades, several well-known NLO crystals, including Li₃O₅ (LBO),¹¹ β-BaB₂O₄ (β-BBO),¹² and KTiOPO₄ (KTP),¹³ have found commercial applications in the UV and visible regions. However, in the IR region, the selection is limited to a few materials, such as AgGaS₂,¹⁴ AgGaSe₂,¹⁵ and ZnGeP₂,¹⁶ which are suitable for the mid-IR range (3–12 μm). These materials are hampered by low

laser damage thresholds (LDT), significantly restricting their utility in laser communication and high-power applications. Compounds that simultaneously exhibit strong second harmonic generation (SHG) effects and broad spectral transmission, from the UV region to the IR region, are exceptionally rare. This rarity stems from the inherent trade-offs between optical properties, such as the band gap and NLO response. Typically, a large SHG response is coupled with a narrow transmission range and low LDT. Thus, balancing the competing demands for a broad transmission range and superior overall optical properties remains a substantial challenge in the development of novel NLO materials.

It is well established that the primary requirement for NLO crystal materials is a non-centrosymmetric (NCS) structure.^{17,18} Thus, designing and synthesizing crystals with NCS structures is of great significance. Recently, metal halides have demonstrated strong potential as NLO materials, largely due to their tendency to form NCS structures, as observed in compounds like Na₂CeF₆¹⁹ and SrCl₂·6H₂O.²⁰ Research studies have indicated that the properties of metal halides are predominantly influenced by the choice of the central metal cation.^{21–26} For instance, selecting metals with stereochemically active lone pairs (SCALP) (e.g., Sn²⁺, Sb³⁺, Bi³⁺, and Pb²⁺) often results in compounds with exceptional NLO properties, as evidenced by Pb₃Mg₃TeP₂O₁₄ (13.5 × KDP),²⁷ Bi(VO₃)₂ (11.5 × KDP),²⁸ and Sn(VO₃)₂ (3 × KDP).²⁹ In this study, we focus on antimony

^aCollege of Chemistry and Materials Science, Sichuan Normal University, Chengdu, 610066, P. R. China. E-mail: huangl026@sina.com

^bCollege of Chemistry, Sichuan University, Chengdu, 610065, P. R. China.
E-mail: zough@scu.edu.cn

† Electronic supplementary information (ESI) available: Detailed crystallographic data, LDT test data, calculation of the single-cell dipole moments, crystal photographs, XRD patterns, TGA curves, UV optical diffuse reflectance spectra and the calculated refractive index for RbSbF₃Cl. CCDC 2387734 and 2375479. For ESI and crystallographic data in CIF or other electronic format see DOI: <https://doi.org/10.1039/d4qi02757d>

halides, building on our recent work with antimony oxysalt NLO crystals. Sb-based cations possess SCALP, which are easily polarizable and can favorably contribute to NLO performance. Additionally, antimony is a relatively robust metal, and its compounds typically exhibit wide band gaps, resulting in high LDT values.³⁰ Compounds such as $\text{K}_2\text{Sb}(\text{P}_2\text{O}_7)\text{F}$ ($4.0 \times \text{KDP}$, 4.74 eV),³¹ CsSb_2SO_4 ($3.0 \times \text{KDP}$, 4.76 eV),³² and $\text{Rb}_2\text{SbFP}_2\text{O}_7$ ($5.1 \times \text{KDP}$, 4.76 eV)³³ have been found to possess a strong SHG response and a broad transmittance range.

To enhance the likelihood of obtaining NCS antimony halide crystals, a common strategy is to modify their structures and properties by introducing mixed halogens. Sb^{3+} cations readily coordinate with halogen atoms (F/Cl/Br/I), forming a variety of irregular geometrical configurations, including SbX_3 triangular pyramids, SbX_4 seesaws, and SbX_5 tetragonal pyramids. By integrating these configurations with different combinations of the four halogen elements, a diverse array of halide compounds with varied structural features can be synthesized. This approach enables the discovery of candidates with excellent comprehensive properties, including significant NLO effects, high LDTs, and broad transparency windows, such as $\text{Cs}_2\text{Hg}_2\text{Br}_2\text{I}_4 \cdot \text{H}_2\text{O}$ ($6 \times \text{KDP}$),³⁴ $\text{Rb}_2\text{CdBr}_2\text{I}_2$ ($4 \times \text{KDP}$),³⁵ and Hg_2BrI_3 ($1.2 \times \text{KTP}$).³⁶

Building on the halogen mixing strategy, two novel antimony-based mixed halide crystals, RbSbF_3Cl and $\text{Rb}_3\text{Sb}_4\text{F}_{14}\text{Cl}$, have been successfully synthesized by combining Sb^{3+} cations with fluorine and chlorine atoms. The two compounds feature NCS structures composed of different Sb-based polyhedra. Remarkably, $\text{Rb}_3\text{Sb}_4\text{F}_{14}\text{Cl}$ exhibits a large SHG response, achieving a value three times higher than that of KDP. It also possesses a broad transparency range of $0.27\text{--}13.3 \mu\text{m}$ and a high LDT of 223 MW cm^{-2} . Meanwhile, RbSbF_3Cl , as a uniaxial crystal, features a high birefringence of 0.31 at 546 nm .

Experimental section

Synthesis of RbSbF_3Cl and $\text{Rb}_3\text{Sb}_4\text{F}_{14}\text{Cl}$

The reaction reagents SbF_3 ($\geq 99.8\%$), Rb_2CO_3 ($\geq 99.0\%$), and HCl (AR grade) were obtained from Aladdin and used without further purification.

The single crystals of both the compounds, RbSbF_3Cl and $\text{Rb}_3\text{Sb}_4\text{F}_{14}\text{Cl}$, were synthesized using an aqueous solution method. The same raw materials of Rb_2CO_3 (0.231 g , 1 mmol) and SbF_3 (0.358 g , 2 mmol) were dissolved in 1 mL of distilled water, to which 0.3 mL and 0.1 mL of HCl (12 mol L^{-1}) were added to obtain RbSbF_3Cl and $\text{Rb}_3\text{Sb}_4\text{F}_{14}\text{Cl}$, respectively. The resulting mixtures were stirred at room temperature for 15 to 20 minutes and then filtered. The filtrates were allowed to evaporate slowly in a refrigerator at 5°C . After two days, colorless and transparent block crystals of RbSbF_3Cl and flake-like crystals of $\text{Rb}_3\text{Sb}_4\text{F}_{14}\text{Cl}$ were collected from the bottom of the plastic beakers (Fig. S1†). The yields of RbSbF_3Cl and $\text{Rb}_3\text{Sb}_4\text{F}_{14}\text{Cl}$ were approximately 38% and 42% , respectively, based on antimony.

Results and discussion

Crystal structure description

RbSbF_3Cl crystallizes in the tetragonal crystal system, belonging to the NCS space group $I\bar{4}2m$ (No. 121) (Tables S1, S2 and S4†).^{37,38} The asymmetric unit comprises one Sb atom, one Rb atom, one Cl atom, and three F atoms. The Sb atom adopts a tetragonal pyramidal geometry as $[\text{SbF}_3\text{Cl}_2]^{2-}$ (I), coordinating with three F atoms and two Cl atoms (Fig. 1a). The Sb–F bond lengths range from 1.917 to 1.962 \AA , while the Sb–Cl bond length measures 2.889 \AA . In this compound, four $[\text{SbF}_3\text{Cl}_2]^{2-}$ (I) units interconnect by sharing four Cl atoms, forming a square-shaped $[\text{Sb}_4\text{F}_{12}\text{Cl}_4]^{4-}$ (II) structure with four-membered rings (4-MR) arranged orderly within the $a\text{-}b$ plane (Fig. 1b). Additionally, Rb^+ ions occupy the cavities of the 4-MR, serving as charge balancers and exhibiting two distinct coordination modes in RbSbF_3Cl . Both Rb1 and Rb2 atoms coordinate with four Cl atoms, while they bind with six and eight F atoms, respectively, resulting in the anionic complexes $[\text{RbF}_6\text{Cl}_4]^{9-}$ and $[\text{RbF}_8\text{Cl}_4]^{11-}$. The Rb–F bond lengths range from 2.974 to 3.562 \AA , while the Rb1–Cl and Rb2–Cl bond lengths are 3.544 \AA and 3.424 \AA , respectively (Fig. S2a†).

$\text{Rb}_3\text{Sb}_4\text{F}_{14}\text{Cl}$ forms crystals in the orthorhombic system's NCS space group $Pmn2_1$ (No. 31) (Tables S1, S3 and S5†). The asymmetric unit comprises four Sb atoms, three Rb atoms, one Cl atom, and fourteen F atoms. In this compound, the three distinct Sb atoms exhibit different coordination environments; $[\text{SbF}_3\text{Cl}_2]^{2-}$ (I) and $[\text{SbF}_5]^{2-}$ (IV) form tetragonal pyramidal configurations, while $[\text{SbF}_4]^-$ (III) adopts a seesaw configuration, with varying numbers of coordinating F and Cl atoms. The Sb–Cl bond length is 2.894 \AA , whereas the Sb–F bond lengths vary from 1.913 to 2.450 \AA . These polyhedra further assemble into structurally distinct clusters. For instance, two $[\text{SbF}_4]^-$ (III) polyhedra share an F atom to form a $[\text{Sb}_2\text{F}_7]^-$ (V) cluster, while a $[\text{Sb}_3\text{F}_{11}]^{2-}$ (VI) cluster is formed by sharing two F atoms among two $[\text{SbF}_4]^-$ (III) units and one $[\text{SbF}_5]^{2-}$ (IV) unit (Fig. 1c). These four clusters are arranged sequentially along the a -axis in the order $[\text{SbF}_3\text{Cl}_2]^{2-}$ (I), $[\text{Sb}_2\text{F}_7]^-$ (V), $[\text{Sb}_3\text{F}_{11}]^{2-}$ (VI), and $[\text{Sb}_2\text{F}_7]^-$ (V), repeating this pattern between adjacent layers (Fig. 1d). Additionally, Rb^+ cations serve as charge balancers and are systematically positioned within the cavities between the Sb-polyhedra, displaying three distinct coordination modes in $\text{Rb}_3\text{Sb}_4\text{F}_{14}\text{Cl}$ (Fig. S2b†). Specifically, Rb1 coordinates with one Cl atom and nine F atoms to form the $[\text{RbF}_9\text{Cl}]^{9-}$ polyhedron, Rb2 coordinates with one Cl atom and ten F atoms to form $[\text{RbF}_{10}\text{Cl}]^{10-}$, and Rb3 coordinates with nine F atoms to form the $[\text{RbF}_9]^{8-}$ polyhedron. The Rb–F bond lengths range from 2.769 to 3.454 \AA , while the Rb1–Cl and Rb2–Cl bond lengths are 3.356 \AA and 3.393 \AA , respectively.

By calculating the bond valence sum (BVS), the validity of the structures of both compounds was confirmed.³⁹ The atomic oxidation states of Rb^+ , Sb^{3+} , F^- , and Cl^- in RbSbF_3Cl and $\text{Rb}_3\text{Sb}_4\text{F}_{14}\text{Cl}$ were determined to be $0.93\text{--}1.15$, $2.90\text{--}3.20$, $0.90\text{--}1.29$, and $0.89\text{--}1.09$, respectively (Tables S2 and S3†).

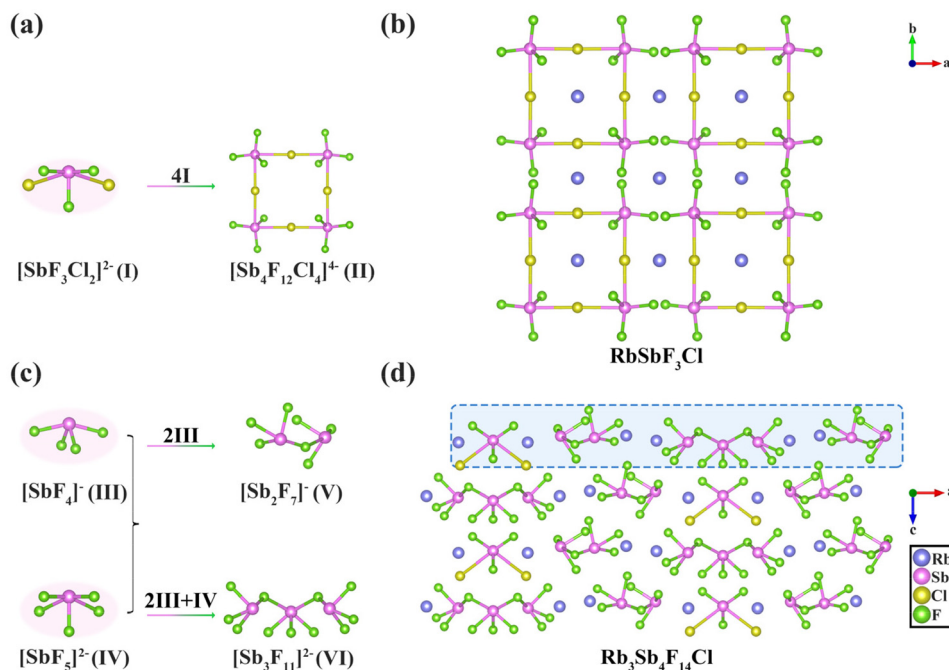


Fig. 1 (a and c) Various coordination patterns and linkage modes of Sb^{3+} . (b) Arrangement of 4-MR and Rb^+ cations in RbSbF_3Cl along the *a*-*b* plane. (d) Arrangement of different Sb polyhedra and Rb^+ cations in $\text{Rb}_3\text{Sb}_4\text{F}_{14}\text{Cl}$.

Powder X-ray diffraction

The phase purity of RbSbF_3Cl and $\text{Rb}_3\text{Sb}_4\text{F}_{14}\text{Cl}$ was verified through powder X-ray diffraction analysis. The experimental data, as presented in Fig. S3,[†] are consistent with the patterns derived from single-crystal X-ray diffraction, confirming that the powder samples are indeed pure phases.

Thermal properties

Thermogravimetric analysis (TGA) was conducted to evaluate the thermal stability of RbSbF_3Cl and $\text{Rb}_3\text{Sb}_4\text{F}_{14}\text{Cl}$. As depicted in Fig. S4,[†] the TGA curves indicate that both the compounds are stable up to approximately 200 °C.

Optical properties

The IR spectra of the two compounds are shown in Fig. 2a, with characteristic absorption bands near 568/513/471 cm^{-1} and 751/572/528/479 cm^{-1} , corresponding to the stretching vibrations of the Sb–F and Sb–Cl bonds. These vibrational modes align with those reported in the literature.^{40,41} The UV-vis-NIR diffuse reflectance spectra of both RbSbF_3Cl and $\text{Rb}_3\text{Sb}_4\text{F}_{14}\text{Cl}$, presented in Fig. 2b and Fig. S5,[†] indicate band gaps of 4.49 and 4.60 eV, corresponding to UV cutoff edges at 276 and 269 nm.⁴² Based on the data from the IR and UV-vis-NIR spectra, the two compounds are transparent across 0.28 to 17.6 and 0.27 to 13.3 μm , respectively, covering short-wave UV to mid-IR regions.

To develop broadband NLO materials, the main group Sb³⁺ cations and F[−] ions were combined to shift the cutoff edge towards shorter wavelengths. The distortion of Sb³⁺ upon coordination promotes asymmetric structures, which may also

enhance SHG response. Additionally, the incorporation of Rb⁺, which lacks d–d and f–f transitions, minimizes electronic absorption in the visible and UV regions, potentially lowering the UV cutoff and extending the transparency range. As a result, the title compounds exhibit short UV cutoffs at 276 and 269 nm. Fig. 2c compares the UV cutoff edges of the title compounds with various metal halides,^{30,35,36,43–54} such as $\text{K}_2\text{SbF}_2\text{Cl}_3$,³⁰ $\text{Cs}_2\text{HgI}_2\text{Cl}_2$,⁴³ and CsSbF_3Cl ,⁴⁴ which have cutoffs at 309 nm, 394 nm, and 405 nm, respectively, and are transparent in the UV range. Unlike most reported metal halides, the two title compounds presented here exhibit broad transmission ranges (0.28–17.6 μm and 0.27–13.3 μm), covering the short-wave UV to mid-IR regions, highlighting their potential as broadband optical materials.

NLO and birefringence properties

The SHG properties of RbSbF_3Cl and $\text{Rb}_3\text{Sb}_4\text{F}_{14}\text{Cl}$ were evaluated using KDP as a reference since they crystallize in the NCS space groups $\bar{I}42m$ and $Pmn2_1$, respectively.⁵⁵ However, the results of the frequency doubling performance of the two compounds vary a lot, with compound RbSbF_3Cl being undetectable due to the small value of the frequency doubling response signal, while $\text{Rb}_3\text{Sb}_4\text{F}_{14}\text{Cl}$ indicates a large SHG response, which is approximately 3 times that of KDP, as depicted in Fig. 3a. Additionally, the SHG signal increases with the increased particle size of the $\text{Rb}_3\text{Sb}_4\text{F}_{14}\text{Cl}$ crystals, suggesting that compound $\text{Rb}_3\text{Sb}_4\text{F}_{14}\text{Cl}$ exhibits type I phase-matching properties (Fig. 3a). The difference in the SHG response of the two compounds was explored, which may be affected by the orientations of the lone pair of electrons of Sb in the unit cell.

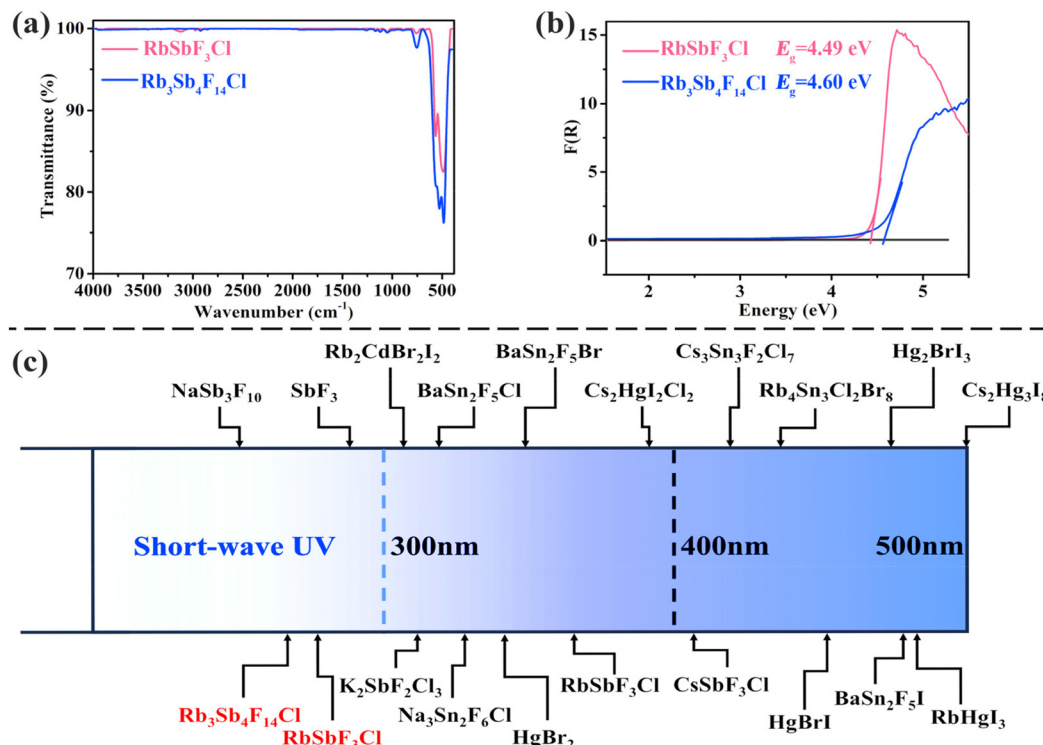


Fig. 2 (a) IR spectra of compounds RbSbF₃Cl and Rb₃Sb₄F₁₄Cl. (b) Band gaps for RbSbF₃Cl and Rb₃Sb₄F₁₄Cl. (c) Comparison of the cutoff edges of RbSbF₃Cl and Rb₃Sb₄F₁₄Cl with those various reported metal halides.

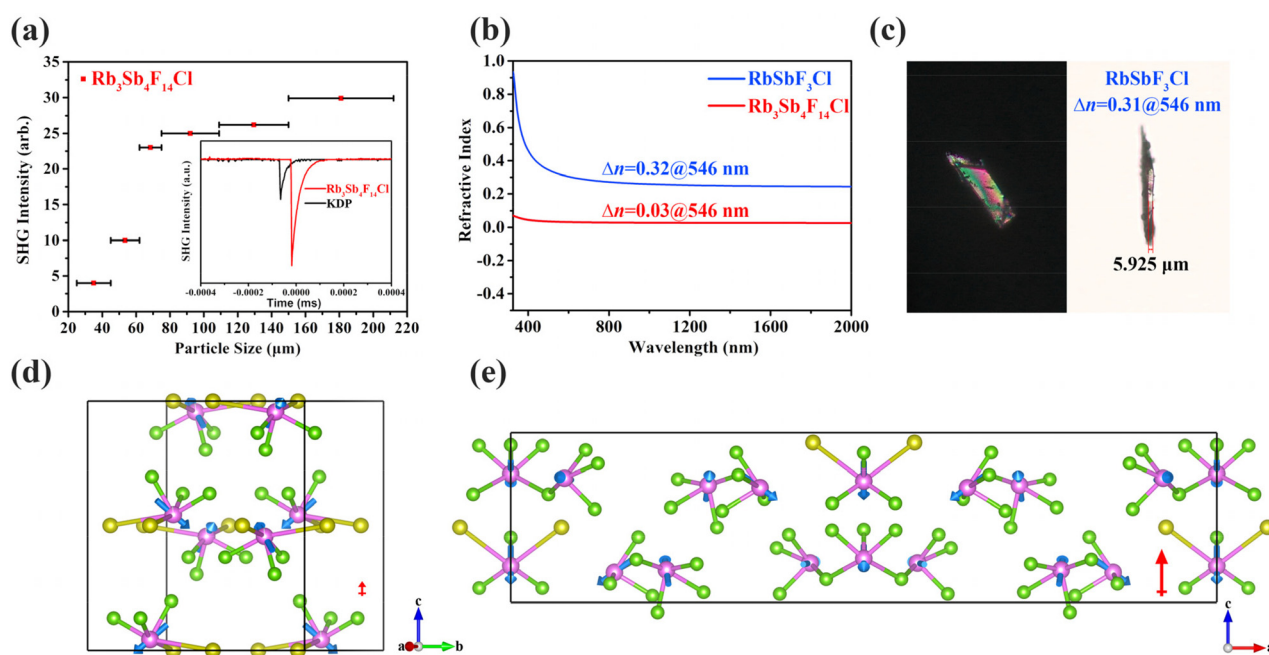


Fig. 3 (a) The phase-matching curve for Rb₃Sb₄F₁₄Cl. Inset: SHG intensity with KDP as the reference (150–212 μm). (b) Calculated birefringence for RbSbF₃Cl and Rb₃Sb₄F₁₄Cl. (c) The experimental birefringence of RbSbF₃Cl. (d) The orientations of the lone pair of electrons in the unit cell of RbSbF₃Cl. (e) The orientations of the lone pair of electrons on Sb³⁺ within a single cell in Rb₃Sb₄F₁₄Cl. The direction of the overall dipole moments is highlighted by a red arrow.

The orientations of the lone pair of electrons in compound **RbSbF₃Cl** are demonstrated in Fig. 3d. By roughly estimating the total dipole moment, due to the nearly opposite orientations of the effective dipole moments of Sb³⁺ ions along the *c*-axis, the contribution of Sb³⁺ cations to the SHG effect is almost entirely canceled out. As a result, the SHG effect of this compound is extremely weak and cannot be detected by instrumentation. However, this arrangement is conducive to the superposition of birefringence, because birefringence is scarcely affected or canceled by the opposite directions of the lone pair of electrons based on current research studies.^{56,57} Hence, **RbSbF₃Cl** exhibits a large experimental birefringence of 0.31@546 nm ascribed to the superposition of the lone pair of electrons of Sb³⁺ along the *c*-axis direction (Fig. 3c).⁵⁸ For the other compound **Rb₃Sb₄F₁₄Cl**, it exhibits a significantly larger SHG effect, approximately three times that of KDP, compared to **RbSbF₃Cl**, which can be attributed to the higher density of Sb³⁺ in the unit cell (Table S6†), despite the relatively disordered orientation of the lone pair of electrons of the central Sb³⁺ cation (Fig. 3e). However, the disordered orientation results in a much smaller calculated birefringence of 0.03 at 546 nm (Fig. 3b). Compared to some SCALP-containing oxy-salts,⁵⁹ such as BiOIO₃⁶⁰ and LiHgPO₄,⁶¹ the title compound **Rb₃Sb₄F₁₄Cl** shows a relatively weaker SHG response but features a significantly shorter UV cutoff edge. This confirms that the mixed halide antimony compounds have potential as broadband second-harmonic generation materials.

LDT measurements

As described above, the band gaps of **RbSbF₃Cl** and **Rb₃Sb₄F₁₄Cl** were found to be 4.49 and 4.60 eV, respectively. Generally, a larger band gap indicates a higher LDT. The LDTs

of the two compounds were tested using a 1064 nm laser with a 10 ns pulse width, resulting in values of 163 and 223 MW cm⁻², respectively, five and seven times higher than that of AgGaS₂ (30 MW cm⁻²) under the same conditions (Table S7†).⁶²

Theoretical calculations

DFT calculations were conducted to investigate the relationship between the structures and optical properties of **RbSbF₃Cl** and **Rb₃Sb₄F₁₄Cl**.⁶³ The birefringence of **RbSbF₃Cl** and **Rb₃Sb₄F₁₄Cl** was calculated to be 0.32 and 0.03 at 546 nm (Fig. 3b), respectively. For that $n_0 > n_e$ in **RbSbF₃Cl**, indicating that it is a uniaxial crystal (Fig. S6†). Furthermore, the theoretical band gaps of **RbSbF₃Cl** and **Rb₃Sb₄F₁₄Cl** were determined to be 3.79 and 4.04 eV, respectively, both of which are 0.70 and 0.56 eV lower than their experimental values (Fig. 4a and b).⁶⁴ These discrepancies align with the well-known tendency of the DFT-GGA approach to underestimate band gaps.⁶⁵ Additionally, the total densities of states (TDOS) and partial densities of states (PDOS) for **RbSbF₃Cl** and **Rb₃Sb₄F₁₄Cl** were computed, offering detailed insights into the contributions of individual atomic orbitals to the energy bands (Fig. 4c and d). For **RbSbF₃Cl**, the upper valence bands, spanning from -10 to 0 eV, are primarily composed of F-2p, Cl-3p, Sb-5p, and Sb-5s orbitals. In contrast, the lower conduction bands, within the energy range of 0 to 10 eV, predominantly consist of Sb-5p, Rb-5s, and Rb-5p orbitals. Similarly, in **Rb₃Sb₄F₁₄Cl**, the valence bands from -10 to 0 eV are primarily made up of F-2p, Rb-5p, Cl-3p, Sb-5s, and Sb-5p orbitals. Moreover, the conduction bands between 0 and 10 eV are largely dominated by Sb-5p and F-2p orbitals. The graphs of the density of states for **RbSbF₃Cl** and **Rb₃Sb₄F₁₄Cl** show a significant overlap

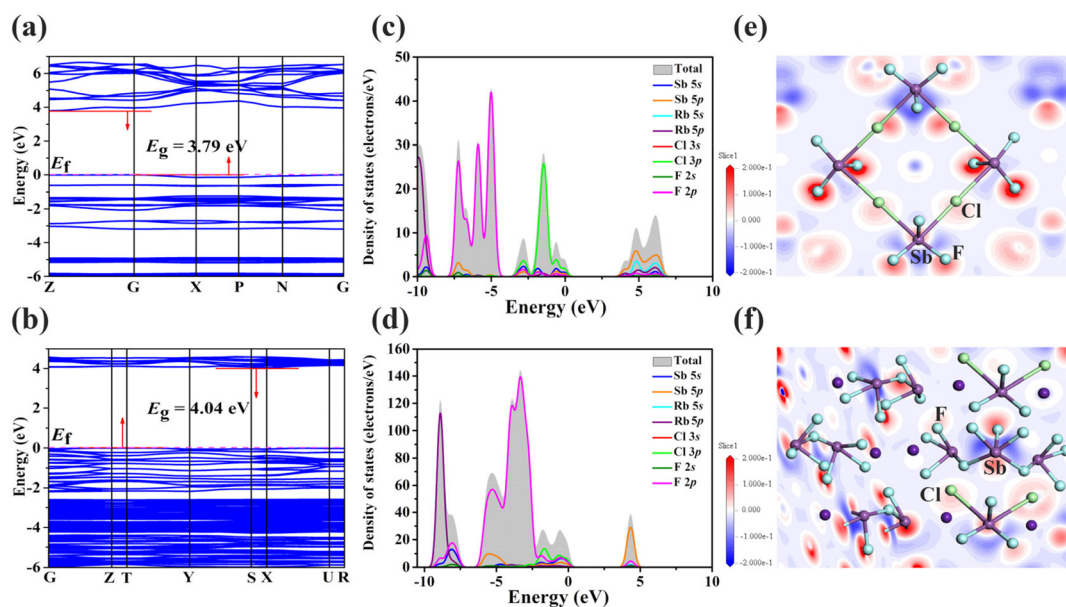


Fig. 4 (a and b) Calculated band structures for **RbSbF₃Cl** and **Rb₃Sb₄F₁₄Cl**. (c and d) The TDOS and PDOS of **RbSbF₃Cl** and **Rb₃Sb₄F₁₄Cl**. (e and f) Electron density difference maps of **RbSbF₃Cl** and **Rb₃Sb₄F₁₄Cl**.

between the Sb-5s and Sb-5p orbitals and the F-2p and Cl-3p orbitals, indicating the presence of Sb-F and Sb-Cl bonds. It is well established that states near the Fermi level play a critical role in determining the NLO properties of a compound. In the case of **RbSbF₃Cl** and **Rb₃Sb₄F₁₄Cl**, the electronic orbitals around the Fermi level include Sb-5s, Sb-5p, F-2p, and Cl-3p, indicating that the optical properties of **RbSbF₃Cl** are primarily influenced by the [SbF₃Cl₂]²⁻ groups, whereas those of **Rb₃Sb₄F₁₄Cl** are mainly influenced by the [SbF₃Cl₂]²⁻, [SbF₄]⁻, and [SbF₅]²⁻ groups. To further validate this inference, dipole moment calculations were performed for both compounds. The results indicate that in **RbSbF₃Cl**, the calculated dipole moment of the [SbF₃Cl₂]²⁻ groups is almost zero (Table S8†). For **Rb₃Sb₄F₁₄Cl**, the local dipole moments of the tetragonal pyramidal [SbF₃Cl₂]²⁻ and [SbF₅]²⁻ units and the seesaw [SbF₄]⁻ unit were calculated to be 35.18 D (Debye), 45.64 D, and 39.71 D along the z-component, respectively, while the x- and y-components of all dipole moments in **Rb₃Sb₄F₁₄Cl** were close to zero (Table S9†). This indicates that all three polyhedra contribute collectively to the NLO performance of **Rb₃Sb₄F₁₄Cl**. Moreover, highly asymmetric lobes observed around the Sb³⁺ cations can be attributed to the presence of lone pairs (Fig. 4e and f).

Conclusions

In this study, we successfully synthesized two NCS compounds, **RbSbF₃Cl** and **Rb₃Sb₄F₁₄Cl**, using a halogen-mixing strategy in a Sb³⁺-containing system. Among these, **Rb₃Sb₄F₁₄Cl** stands out due to its large SHG response, which is approximately 3 times greater than that of KDP. Additionally, it demonstrates high transparency across a wide spectral range, from short-wave UV to mid-IR (0.27 to 13.3 μm), and exhibits a high LDT of 223 MW cm⁻². These remarkable properties make **Rb₃Sb₄F₁₄Cl** a highly promising NLO crystal with superior overall optical performance. Furthermore, **RbSbF₃Cl**, a uniaxial crystal, displays a notable birefringence of approximately 0.31 at 546 nm. This work thus not only presents **Rb₃Sb₄F₁₄Cl** as a new benchmark in advanced NLO crystal design but also highlights the exceptional birefringent characteristics of **RbSbF₃Cl**, demonstrating a promising pathway for the development of next-generation nonlinear optical materials.

Data availability

The authors confirm that the data supporting the findings of this study are available within the article and its ESI.† The authors will supply the relevant data in response to reasonable requests.

Conflicts of interest

The authors declare no competing financial interest.

Acknowledgements

The authors thank Dr Daichuan Ma at the Analytical and Testing Center, Sichuan University, for his valuable technical help in the Material Studio calculations. This work was supported by the National Natural Science Foundation of China (Grant No. 22375139, 22122106, 22071158, 22201195, and 22305166) and the Natural Science Foundation of Sichuan Province (2023NSFSC1066).

References

- Y. Tian, W. Zeng, X. H. Dong, L. Huang, Y. Q. Zhou, H. M. Zeng, Z. E. Lin and G. H. Zou, Enhanced UV Nonlinear Optical Properties in Layered Germanous Phosphites through Functional Group Sequential Construction, *Angew. Chem., Int. Ed.*, 2024, **63**, e202409093.
- G. J. Yi and G. H. Zou, Recent Advances on the Synthesis of Sb(III)-Based Inorganic Ultraviolet Nonlinear Optical Materials, *Chin. J. Struct. Chem.*, 2023, **42**, 100020.
- Y. Q. Li, J. H. Luo and S. G. Zhao, Local Polarity-Induced Assembly of Second-Order Nonlinear Optical Materials, *Acc. Chem. Res.*, 2022, **55**, 3460–3469.
- H. K. Liu, B. B. Zhang and Y. Wang, Second-order nonlinear optical materials with a benzene-like conjugated π system, *Chem. Commun.*, 2020, **56**, 13689–13701.
- J. H. Jiao, M. Zhang and S. L. Pan, Aluminoborates as Nonlinear Optical Materials, *Angew. Chem., Int. Ed.*, 2023, **62**, e202217037.
- J. Cheng, G. J. Yi, Z. Z. Zhang, Y. Long, H. M. Zeng, L. Huang, G. H. Zou and Z. E. Lin, In Situ Chiral Template Approach to Synthesize Homochiral Lead Iodides for Second-Harmonic Generation, *Angew. Chem., Int. Ed.*, 2024, **63**, e202318385.
- H. Y. Sha, Z. Y. Xiong, J. X. Xu, Z. J. Wang, R. B. Su, C. He, X. M. Yang, X. F. Long and Y. Liu, Phosphogermanate Crystal: A New Ultraviolet–Infrared Nonlinear Optical Crystal with Excellent Optical Performances, *ACS Appl. Mater. Interfaces*, 2022, **14**, 10588–10593.
- X. Liu, L. M. Wu, L. Kang, Z. S. Lin and L. Chen, Theoretical Prediction of Monolayer BeP₂O₄H₄ with Excellent Nonlinear–Optical Properties in Deep–Ultraviolet Range, *Small*, 2024, **20**, 2404155.
- Z. Y. Bai and K. M. Ok, Advances in aliovalent substitution strategy for the design and synthesis of nonlinear optical materials: d⁰ transition metal/gallium iodates and selenites, *Coord. Chem. Rev.*, 2023, **490**, 215212.
- J. Song, C. G. Li, J. M. Jiao, Y. H. She, W. L. Zhao, F. Liang, N. Ye, Z. G. Hu and Y. C. Wu, KNa₂La₂(BO₃)₃: a shortite-type lanthanide borate exhibiting strong nonlinear optical activity induced by isolated [BO₃] triangles and distorted [LaO₉] polyhedra, *Inorg. Chem. Front.*, 2023, **10**, 5488–5495.
- C. T. Chen, Y. C. Wu, A. D. Jiang, B. C. Wu, G. M. You, R. K. Li and S. J. Lin, New nonlinear-optical crystal: LiB₃O₅, *J. Opt. Soc. Am. B*, 1989, **6**, 616–621.

12 C. T. Chen, B. C. Wu, A. D. Jiang and G. M. You, A new-type ultraviolet SHG crystal β -BaB₂O₄, *Sci. Sin. (Engl. Ed.)*, 1985, **28**, 235–243.

13 J. D. Bierlein and H. Vanherzele, Potassium Titanyl Phosphate: Properties and New Applications, *J. Opt. Soc. Am. B*, 1989, **6**, 622–633.

14 D. S. Chemla, P. J. Kupcek, D. S. Robertson and R. C. Smith, Silver thiogallate, a new material with potential for infrared devices, *Opt. Commun.*, 1971, **3**, 29–31.

15 G. D. Boyd, H. M. Kasper, J. H. McFee and F. G. Storz, Linear and Nonlinear Optical Properties of Some Ternary Selenides, *IEEE J. Quantum Electron.*, 1972, **8**, 900–908.

16 G. D. Boyd, E. Buehler and F. G. Storz, Linear and Nonlinear Optical Properties of ZnGeP₂ and CdSe, *Appl. Phys. Lett.*, 1971, **18**, 301–304.

17 Y. P. Zhang, S. M. Pei, W. F. Chen, B. W. Liu, X. M. Jiang and G. C. Guo, The centrosymmetric to non-centrosymmetric transformation induced by alkaline-earth cations producing infrared nonlinear optical AeMn₆Ga₆S₁₆ (Ae=Ca, Sr), *Sci. China: Chem.*, 2024, **67**, 2941–2948.

18 T. H. Wu, X. X. Jiang, C. Wu, Z. S. Lin, Z. P. Huang, M. G. Humphrey and C. Zhang, Ce₃F₄(SO₄)₄: cationic framework assembly for designing polar nonlinear optical material through fluorination degree modulation, *Inorg. Chem. Front.*, 2023, **10**, 5270–5277.

19 R. L. Tang, W. Xu, X. Lian, Y. Q. Wei, Y. L. Lv, W. L. Liu and S. P. Guo, Na₂CeF₆: A Highly Laser Damage-Tolerant Double Perovskite Type Ce(IV) Fluoride Exhibiting Strong Second-Harmonic Generation Effect, *Small*, 2024, **20**, 2308348.

20 W. Xu, R. L. Tang, Y. L. Wei, J. M. Wang, Y. Q. Zhang, W. L. Liu and S. P. Guo, SrCl₂·6H₂O: An Alkaline-Earth-Metal Chloride Hexahydrate as Deep-Ultraviolet Nonlinear-Optical Crystal with the $\{[\text{Sr}(\text{H}_2\text{O})_6]^{2+}\}_\infty$ Cationic Framework, *Inorg. Chem.*, 2023, **62**, 10523–10527.

21 Z. Z. Zhang, J. Jin, Y. P. Lin, H. P. Xu, J. Cheng, H. M. Zeng, Z. E. Lin, Z. G. Xia and G. H. Zou, Multisite Fine-Tuning in Hybrid Cadmium Halides Enables Wide Range Emissions for Anti-Counterfeiting, *Angew. Chem., Int. Ed.*, 2024, **63**, e202400760.

22 H. P. Xu, W. Q. Liang, Z. Z. Zhang, C. Cao, W. S. Yang, H. M. Zeng, Z. E. Lin, D. W. Zhao and G. H. Zou, 2D Perovskite Mn²⁺-Doped Cs₂CdBr₂Cl₂ Scintillator for Low-Dose High-Resolution X-ray Imaging, *Adv. Mater.*, 2023, **35**, 2300136.

23 H. B. Wang, J. Z. Li, H. L. Lu, S. Gull, T. Y. Shao, Y. X. Zhang, T. F. He, Y. S. Chen, T. C. He and G. K. Long, Chiral Hybrid Germanium(II) Halide with Strong Nonlinear Chiroptical Properties, *Angew. Chem., Int. Ed.*, 2023, **62**, e202309600.

24 W. Z. Li, X. Mao, H. Yin, Y. X. Wang, Y. F. Wang, J. S. Chen, K. L. Han and R. L. Zhang, Guest-Dependent Stimuli-Responsive Photoluminescence in 0D Antimony Chlorides for Anticounterfeiting and Encryption Applications, *Adv. Funct. Mater.*, 2024, 2413049.

25 X. C. Wang, T. X. Bai, J. L. Sun, J. Y. Liu, Y. Su and J. S. Chen, The effect of solvent on the formation of low-dimensional metal halides and their self-trapped exciton emission, *Chem. Eng. J.*, 2024, **486**, 150257.

26 X. C. Wang, T. X. Bai, J. L. Sun, J. Y. Liu, Y. Su and J. S. Chen, Unlocking Full-Spectrum Brilliance: Dimensional Regulation in Lead-Free Metal Halides for Superior Photoluminescence, *Nano Lett.*, 2024, **24**, 14686–14694.

27 H. W. Yu, W. G. Zhang, J. Young, J. M. Rondinelli and P. S. Halasyamani, Bidenticity-Enhanced Second Harmonic Generation from Pb Chelation in Pb₃Mg₃TeP₂O₁₄, *J. Am. Chem. Soc.*, 2016, **138**, 88–91.

28 F. F. Mao, C. L. Hu, X. Xu, D. Yan, B. P. Yang and J. G. Mao, Bi(IO₃)F₂: The First Metal Iodate Fluoride with a Very Strong Second Harmonic Generation Effect, *Angew. Chem., Int. Ed.*, 2017, **56**, 2151–2155.

29 M. Luo, F. Liang, X. Hao, D. H. Lin, B. X. Li, Z. S. Lin and N. Ye, Rational Design of the Nonlinear Optical Response in a Tin Iodate Fluoride Sn(IO₃)₂F₂, *Chem. Mater.*, 2020, **32**, 2615–2620.

30 Y. Huang, X. G. Meng, P. F. Gong, Z. S. Lin, X. G. Chen and J. G. Qin, A study on K₂SbF₂Cl₃ as a new mid-IR nonlinear optical material: new synthesis and excellent properties, *J. Mater. Chem. C*, 2015, **3**, 9588–9593.

31 Y. L. Deng, L. Huang, X. H. Dong, L. Wang, K. M. Ok, H. M. Zeng, Z. E. Lin and G. H. Zou, K₂Sb(P₂O₇)F: Cairo Pentagonal Layer with Bifunctional Genes Reveal Optical Performance, *Angew. Chem., Int. Ed.*, 2020, **59**, 21151–21156.

32 X. H. Dong, L. Huang, C. F. Hu, H. M. Zeng, Z. E. Lin, X. Wang, K. M. Ok and G. H. Zou, CsSbF₂SO₄: An Excellent Ultraviolet Nonlinear Optical Sulfate with a KTiOPO₄ (KTP)-type Structure, *Angew. Chem., Int. Ed.*, 2019, **58**, 6528–6534.

33 X. H. Dong, H. B. Huang, L. Huang, Y. Q. Zhou, B. B. Zhang, H. M. Zeng, Z. E. Lin and G. H. Zou, Unearthing Superior Inorganic UV Second-Order Nonlinear Optical Materials: A Mineral-Inspired Method Integrating First-Principles High-Throughput Screening and Crystal Engineering, *Angew. Chem., Int. Ed.*, 2024, **63**, e202318976.

34 Q. Wu, Y. Huang, X. G. Meng, C. Zhong, X. G. Chen and J. G. Qin, Exploration of new second-order nonlinear optical materials of the Cs–Hg–Br–I system, *Dalton Trans.*, 2014, **43**, 8899–8904.

35 Q. Wu, X. G. Meng, C. Zhong, X. G. Chen and J. G. Qin, Rb₂CdBr₂I₂: A New IR Nonlinear Optical Material with a Large Laser Damage Threshold, *J. Am. Chem. Soc.*, 2014, **136**, 5683–5686.

36 Y. J. Li, M. Wang, T. X. Zhu, X. G. Meng, C. Zhong, X. G. Chen and J. G. Qin, Synthesis, crystal structure and properties of a new candidate for nonlinear optical material in the IR region: Hg₂BrI₃, *Dalton Trans.*, 2012, **41**, 763–766.

37 G. M. Sheldrick, A short history of SHELX, *Acta Crystallogr., Sect. A: Found. Crystallogr.*, 2008, **64**, 112–122.

38 A. L. Spek, Single-crystal structure validation with the program PLATON, *J. Appl. Crystallogr.*, 2003, **36**, 7–13.

39 I. D. Brown and D. Altermatt, Bond-Valence Parameters Obtained from a Systematic Analysis of the Inorganic Crystal Structure Database, *Acta Crystallogr., Sect. B: Struct. Sci.*, 1985, **41**, 244–247.

40 P. Zhang, X. Mao, X. H. Dong, L. Huang, L. L. Cao, D. J. Gao and G. H. Zou, Two UV Organic-Inorganic Hybrid Antimony-Based Materials with Superior Optical Performance Derived from Cation-Anion Synergetic Interactions, *Chin. Chem. Lett.*, 2024, **35**, 109235.

41 Q. Wang, J. X. Ren, D. Wang, L. L. Cao, X. H. Dong, L. Huang, D. J. Gao and G. H. Zou, Low temperature molten salt synthesis of noncentrosymmetric $(\text{NH}_4)_3\text{SbF}_3(\text{NO}_3)_3$ and centrosymmetric $(\text{NH}_4)_3\text{SbF}_4(\text{NO}_3)_2$, *Inorg. Chem. Front.*, 2023, **10**, 2107–2114.

42 P. Kubelka, Ein Beitrag zur Optik der Farbanstriche, *Z. Tech. Phys.*, 1931, **12**, 593–601.

43 G. Zhang, Y. J. Li, K. Jiang, H. Y. Zeng, T. Liu, X. G. Chen, J. G. Qin, Z. S. Lin, P. Z. Fu, Y. C. Wu and C. T. Chen, A New Mixed Halide, $\text{Cs}_2\text{HgI}_2\text{Cl}_2$: Molecular Engineering for a New Nonlinear Optical Material in the Infrared Region, *J. Am. Chem. Soc.*, 2012, **134**, 14818–14822.

44 P. F. Gong, Y. Yang, F. G. You, X. Y. Zhang, G. M. Song, S. Z. Zhang, Q. Huang and Z. S. Lin, ASbF_3Cl (A = Rb, Cs): Structural Evolution from Centrosymmetry to Noncentrosymmetry, *Cryst. Growth Des.*, 2019, **19**, 1874–1879.

45 G. Zhang, J. G. Qin, T. Liu, Y. J. Li, Y. C. Wu and C. T. Chen, $\text{NaSb}_3\text{F}_{10}$: A new second-order nonlinear optical crystal to be used in the IR region with very high laser damage threshold, *Appl. Phys. Lett.*, 2009, **95**, 261104.

46 G. Zhang, T. Liu, T. X. Zhu, J. G. Qin, Y. C. Wu and C. T. Chen, SbF_3 : A new second-order nonlinear optical material, *Opt. Mater.*, 2008, **31**, 110–113.

47 Z. S. Lin, P. F. Gong, Y. Yang, S. Y. Luo, F. Liang and X. X. Jiang, Structural Evolution in $\text{BaSn}_2\text{F}_5\text{X}$ (X = Cl, Br, I): A Family of Alkaline Earth Metal Tin Mixed Halides, *Inorg. Chem.*, 2017, **56**, 13593–13599.

48 P. F. Gong, S. Y. Luo, K. Xiao, Q. Huang, Y. Yang, H. W. Huang, Y. C. Wu, C. T. Chen and Z. S. Lin, Structure and Characterization of a Zero-Dimensional Alkali Tin Dihalides Compound $\text{Cs}_3\text{Sn}_3\text{F}_2\text{Cl}_7$ with the $[\text{Sn}_2\text{F}_2\text{Cl}_4]^{2-}$ Clusters, *Inorg. Chem.*, 2017, **56**, 3081–3086.

49 P. F. Gong, S. Y. Luo, Y. Yang, F. Liang, S. Z. Zhang, S. G. Zhao, J. H. Luo and Z. S. Lin, Nonlinear Optical Crystal $\text{Rb}_4\text{Sn}_3\text{Cl}_2\text{Br}_8$: Synthesis, Structure, and Characterization, *Cryst. Growth Des.*, 2018, **18**, 380–385.

50 G. Zhang, J. G. Qin, T. Liu, T. X. Zhu, P. Z. Fu, Y. C. Wu and C. T. Chen, Synthesis, Characterization, and Crystal Growth of $\text{Cs}_2\text{Hg}_3\text{I}_6$: A New Second-Order Nonlinear Optical Material, *Cryst. Growth Des.*, 2008, **8**, 2946–2949.

51 P. F. Gong, S. Y. Luo, Q. Huang, Y. Yang, X. X. Jiang, F. Liang, C. T. Chen and Z. S. Lin, An alkaline tin(II) halide compound $\text{Na}_3\text{Sn}_2\text{F}_6\text{Cl}$: Synthesis, structure, and characterization, *J. Solid State Chem.*, 2017, **248**, 104–108.

52 M. S. Zhang, W. D. Yao, S. M. Pei, B. W. Liu, X. M. Jiang and G. C. Guo, HgBr_2 : an easily growing wide-spectrum birefringent crystal, *Chem. Sci.*, 2024, **15**, 6891–6896.

53 Q. Wu, Y. J. Li, H. C. Chen, K. Jiang, H. Li, C. Zhong, X. G. Chen and J. G. Qin, HgBrI : A Promising Nonlinear Optical Material in IR region, *Inorg. Chem. Commun.*, 2013, **34**, 1–3.

54 Y. J. Li, Y. X. Ding, Y. M. Li, H. M. Liu, X. G. Meng, Y. Cong, J. Zhang, X. K. Li, X. G. Chen and J. G. Qin, Synthesis, Crystal Structure and Nonlinear Optical Property of RbHgI_3 , *Crystals*, 2017, **7**, 148.

55 S. K. Kurtz and T. T. Perry, A Powder Technique for the Evaluation of Nonlinear Optical Materials, *J. Appl. Phys.*, 1968, **39**, 3798–3813.

56 J. Y. Guo, J. B. Huang, A. Tudi, X. L. Hou, S. J. Han, Z. H. Yang and S. L. Pan, Birefringence Regulation by Clarifying the Relationship Between Stereochemically Active Lone Pairs and Optical Anisotropy in Tin-based Ternary Halides, *Angew. Chem., Int. Ed.*, 2023, **62**, e202304238.

57 C. Wu, X. X. Jiang, Z. J. Wang, L. Lin, Z. S. Lin, Z. P. Huang, X. F. Long, M. G. Humphrey and C. Zhang, Giant optical anisotropy in the UV-transparent 2D nonlinear optical material $\text{Sc}(\text{IO}_3)_2(\text{NO}_3)$, *Angew. Chem., Int. Ed.*, 2021, **60**, 3464–3468.

58 J. Y. Guo, A. Tudi, S. J. Han, Z. H. Yang and S. L. Pan, $\text{Sn}_2\text{PO}_4\text{I}$: An Excellent Birefringent Material with Giant Optical Anisotropy in Non π -Conjugated Phosphate, *Angew. Chem., Int. Ed.*, 2021, **60**, 24901–24904.

59 J. Chen, C. L. Hu, F. Kong and J. G. Mao, High-Performance Second-Harmonic-Generation (SHG) Materials: New Developments and New Strategies, *Acc. Chem. Res.*, 2021, **54**, 2775–2783.

60 S. D. Nguyen, J. Yeon, S. H. Kim and P. S. Halasyamani, $\text{BiO}(\text{IO}_3)$: A New Polar Iodate that Exhibits an Aurivillius-Type $(\text{Bi}_2\text{O}_2)^{2+}$ Layer and a Large SHG Response, *J. Am. Chem. Soc.*, 2011, **133**, 12422–12425.

61 B. L. Wu, C. L. Hu, F. F. Mao, R. L. Tang and J. G. Mao, Highly Polarizable Hg^{2+} Induced a Strong Second Harmonic Generation Signal and Large Birefringence in LiHgPO_4 , *J. Am. Chem. Soc.*, 2019, **141**, 10188–10192.

62 G. C. Catella and D. Burlage, Crystal growth and optical properties of AgGaS_2 and AgGaSe_2 , *MRS Bull.*, 1998, **23**, 28–36.

63 M. D. Segall, P. J. D. Lindan, M. J. Probert, C. J. Pickard, P. J. Hasnip, S. J. Clark and M. C. Payne, First-principles simulation: ideas, illustrations and the CASTEP code, *J. Phys.: Condens. Matter*, 2002, **14**, 2717–2744.

64 Y. Lan, J. X. Ren, P. Zhang, X. H. Dong, L. Huang, L. L. Cao, D. J. Gao and G. H. Zou, $\text{ASb}(\text{SO}_4)_2$ (A = Rb, Cs): Two short-wave UV antimony sulfates exhibiting large birefringence, *Chin. Chem. Lett.*, 2024, **35**, 108652.

65 J. P. Perdew, K. Burke and M. Ernzerhof, Generalized Gradient Approximation Made Simple, *Phys. Rev. Lett.*, 1996, **77**, 3865–3868.